



<b>Publication Year</b>	2018
<b>Acceptance in OA</b>	2022-07-14T14:51:57Z
<b>Title</b>	VizieR Online Data Catalog: Highly Accreting Quasars: SDSS Low z Catalog (Negrete+, 2018)
<b>Authors</b>	Negrete, C. A., Dultzin, D., MARZIANI, Paola, Esparza, D., Sulentic, J. W., Del Olmo, A., Martinez-Aldama, M. L., Garcia-Lopez, A., D'Onofrio, M., Bon, N.
<b>Publisher's version (DOI)</b>	10.26093/cds/vizieR.36200118
<b>Handle</b>	<a href="http://hdl.handle.net/20.500.12386/32496">http://hdl.handle.net/20.500.12386/32496</a>
<b>Journal</b>	VizieR Online Data Catalog


**J/A+A/620/A118** Highly Accreting Quasars: SDSS Low z Catalog (Negrete+, 2018)

Highly accreting quasars: The SDSS low-redshift catalog.

Negrete C.A., Dultzin D., Marziani P., Esparza D., Sulentic J. W., del Olmo A., Martínez-Aldama M. L., García-López A., D'Onofrio M, Bon N. Bon E.  
<Astron. Astrophys. 620, A118 (2018)>  
=[2018A&A...620A.118N](#) (SIMBAD/NED BibCode)

**ADC\_Keywords:** Surveys ; QSOs ; Redshifts ; Spectroscopy

**Keywords:** catalogs - galaxies: active - galaxies: distances and redshifts - galaxies: nuclei - quasars: emission lines - quasars: general

**Abstract:**

The most highly accreting quasars are of special interest in studies of the physics of active galactic nuclei (AGNs) and host galaxy evolution. Quasars accreting at high rates ( $L/L_{\text{Edd}}-1$ ) hold promise for use as "standard candles": distance indicators detectable at very high redshift. However, their observational properties are still largely unknown.

We seek to identify a significant number of extreme accretors. A large sample can clarify the main properties of quasars radiating near  $L/L_{\text{Edd}}-1$  (in this paper they are designated as extreme Population A quasars or simply as extreme accretors) in the  $H\beta$  spectral range for redshift  $\leq 0.8$ .

We use selection criteria derived from four-dimensional Eigenvector 1 (4DE1) studies to identify and analyze spectra for a sample of 334 candidate sources identified from the SDSS DR7 database. The source spectra were chosen to show a ratio  $R_{\text{FeII}}$  between the FeII emission blend at  $\lambda 4570$  and  $H\beta$ ,  $R_{\text{FeII}} > 1$ . Composite spectra were analyzed for systematic trends as a function of FeII strength, line width, and [OIII] strength. We introduced tighter constraints on the signal-to-noise ratio (S/N) and  $R_{\text{FeII}}$  values that allowed us to isolate sources most likely to be extreme accretors.

We provide a database of detailed measurements. Analysis of the data allows us to confirm that  $H\beta$  shows a Lorentzian function with a full width at half maximum (FWHM) of  $H\beta \leq 4000 \text{ km/s}$ . We find no evidence for a discontinuity at  $2000 \text{ km/s}$  in the 4DE1, which could mean that the sources below this FWHM value do not belong to a different AGN class. Systematic [OIII] blue shifts, as well as a blueshifted component in  $H\beta$  are revealed. We interpret the blueshifts as related to the signature of outflowing gas from the quasar central engine. The FWHM of  $H\beta$  is still affected by the blueshifted emission; however, the effect is non-negligible if the FWHM  $H\beta$  is used as a "virial broadening estimator" (VBE). We emphasize a strong effect of the viewing angle on  $H\beta$  broadening, deriving a correction for those sources that shows major disagreement between virial and concordance cosmology luminosity values.

The relatively large scatter between concordance cosmology and virial luminosity estimates can be reduced (by an order of magnitude) if a correction for orientation effects is included in the FWHM  $H\beta$  value; outflow and sample definition yield relatively minor effects.

**Description:**

Table 4: contains 103 spectra with an erroneous  $z$  identification. The redshift values are given by: the SDSS database (erroneous values), Shen et al. (2011, Cat. [J/ApJS/194/45](#)) and Hewett & Wilde (2010, Cat. [J/MNRAS/405/2302](#)) (correct values).

Table 5: Contains the data described in the Table 2, which are the measurements of the individual spectral fits and derived computations. A detailed description of this table is in Sec. 4.2.

**File Summary:**

FileName	Lrecl	Records	Explanations
ReadMe	80	.	This file
<a href="#">table1.dat</a>	51	101	Objects with an erroneous $z$ identification
<a href="#">table2.dat</a>	543	302	Measurements of the individual spectral fits

**See also:**

[J/MNRAS/405/2302](#) : Improved redshifts for SDSS quasar spectra (Hewett+, 2010)  
[J/ApJS/194/45](#) : QSO properties from SDSS-DR7 (Shen+, 2011)

**Byte-by-byte Description of file:** [table1.dat](#)

Bytes	Format	Units	Label	Explanations
1- 19	A19	---	SDSS	SDSS Name
21- 27	F7.5	---	zSDSS	SDSS DR7 redshift
29- 35	F7.5	---	e_zSDSS	SDSS redshift error
37- 43	F7.5	---	zShen	Shen et al. (2011, Cat. <a href="#">J/ApJS/194/45</a> ) redshift
45- 51	F7.5	---	zHW	Hewitt & Wilde (2010, Cat. <a href="#">J/MNRAS/405/2302</a> ) redshift

Byte-by-byte Description of file: [table2.dat](#)

Bytes	Format	Units	Label	Explanations
1- 19	A19	---	SDSS	SDSS DR7 designation
21- 27	F7.5	---	z	Redshift considered in this work ( <a href="#">1</a> ).
29- 35	F7.5	---	e_z	Redshift error
37- 43	F7.5	---	zSDSS	Redshift SDSS DR7
45- 51	F7.5	---	e_zSDSS	Redshift SDSS DR7 error
53- 57	F5.2	---	S/N	S/N ratio measured around 5100Å
59- 62	F4.2	<a href="#">10-19W/m2/nm</a>	C5100	Continuum flux at 5100Å in $10^{-17}\text{erg/cm}^2/\text{s}/\text{Å}$
64- 67	F4.2	<a href="#">10-19W/m2/nm</a>	e_C5100	Continuum flux at 5100Å error
69- 73	F5.1	---	N5100	Continuum normalization at 5100Å
75- 79	F5.2	---	e_N5100	Continuum normalization at 5100Å error
81- 85	F5.2	---	alpha	Power law index
87- 90	F4.2	---	e_alpha	Power law index error
92	I1	---	FaintHG	Faint contribution of the HG
94-101	F8.2	<a href="#">10-20W/m2</a>	FHbBC	H $\beta$ <sub>BC</sub> line flux in $10^{-17}\text{erg/cm}^2/\text{s}$
103-109	F7.2	<a href="#">10-20W/m2</a>	e_FHbBC	H $\beta$ <sub>BC</sub> line flux error
111-115	F5.2	<a href="#">0.1nm</a>	EWbBC	H $\beta$ <sub>BC</sub> rest-frame equivalent width
117-121	F5.2	<a href="#">0.1nm</a>	e_EWbBC	H $\beta$ <sub>BC</sub> rest-frame equivalent width error
123-127	I5	<a href="#">km/s</a>	ShiftHbBC	H $\beta$ <sub>BC</sub> shift with respect to the rest-frame
129-133	F5.1	<a href="#">km/s</a>	e_ShiftHbBC	H $\beta$ <sub>BC</sub> shift with respect to the rest-frame error
135-142	F8.3	<a href="#">km/s</a>	FWHMHbBC	H $\beta$ <sub>BC</sub> FWHM
144-151	F8.3	<a href="#">km/s</a>	e_FWHMHbBC	H $\beta$ <sub>BC</sub> FWHM error
153	A1	---	Hbprofile	[GL] G = Gaussian, L = Lorentzian
155-161	F7.2	<a href="#">10-20W/m2</a>	FHbblue	H $\beta$ BLUE Line Flux
163-168	F6.2	<a href="#">10-20W/m2</a>	e_FHbblue	H $\beta$ BLUE Line Flux error
170-174	F5.2	<a href="#">0.1nm</a>	EWbblue	H $\beta$ BLUE rest-frame equivalent width
176-179	F4.2	<a href="#">0.1nm</a>	e_EWbblue	H $\beta$ BLUE rest-frame equivalent width error
181-188	F8.2	<a href="#">km/s</a>	ShiftHbblue	H $\beta$ BLUE shift
190-196	F7.2	<a href="#">km/s</a>	e_ShiftHbblue	H $\beta$ BLUE shift error
198-201	I4	<a href="#">km/s</a>	FWHMHbblue	H $\beta$ BLUE FWHM
203-206	I4	<a href="#">km/s</a>	e_FWHMHbblue	H $\beta$ BLUE FWHM error
208-215	F8.2	<a href="#">10-20W/m2</a>	FFeII	FeII flux
217-223	F7.2	<a href="#">10-20W/m2</a>	e_FFeII	FeII flux error
225-230	F6.2	<a href="#">0.1nm</a>	EWFeII	FeII rest-frame equivalent width
232-235	F4.1	<a href="#">0.1nm</a>	e_EWFeII	FeII rest-frame equivalent width error
237-240	A4	---	Pop	Population designation
242-246	F5.3	---	RFeII	Ratio between the FeII emission blend at $\lambda 4570$ and H $\beta$
248-252	F5.3	---	e_RFeII	RFeII error
254-259	F6.3	---	AIHb	H $\beta$ asymetry (only objects with Hbblue)
261-265	F5.3	---	e_AIHb	H $\beta$ asymetry error
267-270	F4.2	---	Kurt	Kurtosis
272-275	F4.2	---	e_Kurt	Kurtosis error
277-281	I5	<a href="#">km/s</a>	C010	H $\beta$ centroid at 0.10 of the line intensity
283-286	I4	<a href="#">km/s</a>	e_C010	H $\beta$ centroid at 0.10 of the line intensity error
288-291	I4	<a href="#">km/s</a>	C025	H $\beta$ centroid at 0.25 of the line intensity
293-295	I3	<a href="#">km/s</a>	e_C025	H $\beta$ centroid at 0.25 of the line intensity error
297-300	I4	<a href="#">km/s</a>	C050	H $\beta$ centroid at 0.50 of the line intensity
302-304	I3	<a href="#">km/s</a>	e_C050	H $\beta$ centroid at 0.50 of the line intensity error
306-309	I4	<a href="#">km/s</a>	C075	H $\beta$ centroid at 0.75 of the line intensity
311-313	I3	<a href="#">km/s</a>	e_C075	H $\beta$ centroid at 0.75 of the line intensity error
315-318	I4	<a href="#">km/s</a>	C090	H $\beta$ centroid at 0.90 of the line intensity
320-322	I3	<a href="#">km/s</a>	e_C090	H $\beta$ centroid at 0.90 of the

				line intensity error
324-329	F6.2	<a href="#">10-20W/m2</a>	FHeII	HeII line flux
331-335	F5.2	<a href="#">10-20W/m2</a>	e_FHeII	HeII line flux error
337-344	F8.2	<a href="#">km/s</a>	ShiftHeII	HeII shift with respect to the rest frame
346-352	F7.2	<a href="#">km/s</a>	e_ShiftHeII	HeII shift with respect to the rest frame error
354-357	I4	<a href="#">km/s</a>	FWHMHeII	HeII FWHM
359-362	I4	<a href="#">km/s</a>	e_FWHMHeII	HeII FWHM error
364-369	F6.2	<a href="#">10-20W/m2</a>	FHbNC	H $\beta$ <sub>NC</sub> Line Flux
371-375	F5.2	<a href="#">10-20W/m2</a>	e_FHbNC	H $\beta$ <sub>NC</sub> Line Flux error
377-380	F4.2	<a href="#">0.1nm</a>	EWbNC	H $\beta$ <sub>NC</sub> rest-frame equivalent width
382-385	F4.2	<a href="#">0.1nm</a>	e_EWbNC	H $\beta$ <sub>NC</sub> rest-frame equivalent width error
387-388	I2	<a href="#">km/s</a>	ShiftHbNC	H $\beta$ <sub>NC</sub> shift with respect to the rest-frame
390-394	F5.1	<a href="#">km/s</a>	e_ShiftHbNC	H $\beta$ <sub>NC</sub> shift with respect to the rest-frame error
396-399	I4	<a href="#">km/s</a>	FWHMHbNC	H $\beta$ <sub>NC</sub> FWHM
401-403	I3	<a href="#">km/s</a>	e_FWHMHbNC	H $\beta$ <sub>NC</sub> FWHM error
405-411	F7.2	<a href="#">10-20W/m2</a>	FOIII	Line flux of [OIII] 5007
413-419	F7.2	<a href="#">10-20W/m2</a>	e_FOIII	Line flux error of [OIII] 5007
421-425	F5.2	<a href="#">0.1nm</a>	EWOIII	Line [OIII] 5007 rest-frame equivalent width
427-431	F5.2	<a href="#">0.1nm</a>	e_EWOIII	Line [OIII] 5007 rest-frame equivalent width error
433-440	F8.2	<a href="#">km/s</a>	ShiftOIII	Line [OIII] 5007 shift with respect to the rest-frame
442-447	F6.2	<a href="#">km/s</a>	e_ShiftOIII	Line [OIII] 5007 shift with respect to the rest-frame error
449-452	I4	<a href="#">km/s</a>	FWHMOIII	Line [OIII] 5007 FWHM
454-457	I4	<a href="#">km/s</a>	e_FWHMOIII	Line [OIII] 5007 FWHM error
459-465	F7.2	<a href="#">10-20W/m2</a>	FOIIISB	Semi broad line [OIII] 5007 flux
467-473	F7.2	<a href="#">10-20W/m2</a>	e_FOIIISB	Semi broad line [OIII] 5007 flux error
475-479	F5.2	<a href="#">0.1nm</a>	EWOIIISB	Semi broad line [OIII] 5007 rest-frame equivalent width
481-485	F5.2	<a href="#">0.1nm</a>	e_EWOIIISB	Semi broad line [OIII] 5007 rest-frame equivalent width error
487-494	F8.2	<a href="#">km/s</a>	ShiftOIIISB	Semi broad line [OIII] 5007 shift with respect to the rest frame
496-501	F6.2	<a href="#">km/s</a>	e_ShiftOIIISB	Semi broad line [OIII] 5007 shift with respect to the rest frame error
503-506	I4	<a href="#">km/s</a>	FWHMOIIISB	Semi broad line [OIII] 5007 FWHM
508-511	I4	<a href="#">km/s</a>	e_FWHMOIIISB	Semi broad line [OIII] 5007 FWHM error
513-516	F4.2	<a href="#">[Msun]</a>	logMBH	Black hole mass
518-521	F4.2	<a href="#">[Msun]</a>	e_logMBH	Black hole mass error
523-527	F5.2	<a href="#">[Lsun]</a>	logLbol	Bolometric luminosity
529-532	F4.2	<a href="#">[Lsun]</a>	e_logLbol	Bolometric luminosity error
534-538	F5.2	---	L/LEdd	Eddington ratio
540-543	F4.2	---	e_L/LEdd	Eddington ratio error

**Note (1):** measured using the H $\beta$ <sub>NC</sub> or [OIII] $\lambda$ 5007 line (see text).

#### Acknowledgements:





Alenka Negrete, alenka(at)astro.unam.mx

(End)

Patricia Vannier [CDS] 10-Sep-2018

The document above follows the rules of the [Standard Description for Astronomical Catalogues](#); from this documentation it is possible to generate *f77* program to load files [into arrays](#) or [line by line](#)

© Université de Strasbourg/CNRS

    [Contact](#) 